Owen, R.B., Sandhu, N., 2000. Heavy metal accumulation and anthropogenic impacts on Tolo Harbour, Hong Kong. Mar. Pollut. Bull. 40, 174–180.

Park, Y.-U, Paeung, W.-H., Hyun, S., 2004. Geochemical characteristics and sedimentary environments of surface sediments in Masan Bay, Korea. Proc. Kor. Soc. Oceanogr. p. 395.

Reish, D.J., 1972. The use of marine invertebrates as indicators of varying degrees of marine pollution. In: Ruivo, M. (Ed.), Marine Pollution and Sea Life. Fishing News Books, London, UK, pp. 203–207.

Ricken, W., 1993. Sedimentation as a Three-Component System, Organic Carbon, Carbonate, Noncarbonate. Springer-Verlag, Berlin, p. 211.

Rubio, B., Nombela, M.A., Vilas, F., 2000. Geochemistry of major and tracer elements in sediments of the Ria de Vigo (NW Spain): an assessment of metal pollution. Mar. Pollut. Bull. 40, 968–980.

Salomons, W., Förstner, U., 1984. Metal in the Hydrocycle. Springer-Verlag, Berlin, p. 349.

Shin, P.K.S., Lam, W.K.C., 2001. Development of a marine sediment pollution index. Environ. Pollut. 113, 281–291.

SNU, 1999. Methodologies for the quality assessment of benthic environment of Korean Costal water. Report of Marine Environmental Monitoring and assessment Technology, Seoul National University (SNU), p. 786.

Sohlenius, G., Emeis, K.-C., Andrén, E., Andrén, T., Kohly, A., 2001. Development of anoxia during the Holocene fresh-brackish water transition in the Baltic Sea. Mar. Geol. 177, 221–242.

Soares, H.M.V.M., Boaventura, R.A.R., Machado, A.A.S.C., Esteves da Silva, J.C.G., 1999. Sediments as monitors of heavy metal contamination in the Ave river basin (Portugal): multivariate analysis of data. Environ. Pollut. 105, 311–323.

Soto-Jimenes, M.F., Paez-Osuna, F., Ruiz-Fernandez, A.C., 2003. Geochemical evidences of the anthropogenic alternation of trace metal composition of the sediments of Chiricahueto marsh (SE Culf of California). Environ. Pollut. 125, 423–432.

Spencer, K.L., Cundy, A.B., Croudace, I.W., 2003. Heavy metal distribution and early diagenesis in salt marsh sediments from the Medway Estuary, Kent, UK. Estuar. Coast. Shelf S. 57, 43–54.

Szefer, P., Kaliszan, R., 1993. Distribution of elements in sediment cores of the Southern Baltic from the point of view of principal component analysis. Studia 1 Materialy Oceanogeczne NR 64. Mar. Pollut. 1, 95–102.

Vogt, N.B., 1990. Multivariate ecotoxicological mapping of the relationships between sediment chemical composition and fauna diversity. Sci. Total Environ. 90, 149–161.

Woo, H.-J., Cho, J.-H., Jeong, K.-S., Chung, C.-S., Kwon, S.-J., Park, S.-M., 2003. Pollution history of the Masan Bay, southeast Korea, from heavy metals and foraminifera in the subsurface sediments. J. Korean Earth Sci. Soc. 24, 635–649 (in Korean with English abstract).

Yim, U.H., Hong, S.H., Shim, W.J., Oh, J.R., Chang, M., 2005. Spatiotemporal distribution and characteristic s of PAHs in sediments from Masan Bay, Korea. Mar. Pollut. Bull. 50, 319–326.

Yokoyama, H., 1995. Macrobenthic assemblages in Omura Bay-1. Community parameters versus bottom environmental factors. Bull. Natl. Res. Inst. Aquacult. 24, 43–53 (in Japanese with English abstract).

Zhang, J., Liu, C.L., 2002. Riverine composition and estuarine geochemistry of particulate metals in China weathering features, anthropogenic impact and chemical fluxes. Estuar. Coast. Shelf S. 54, 1051–1070.

0025-326X/$ - see front matter © 2007 Elsevier Ltd. All rights reserved.
doi:10.1016/j.marpolbul.2007.02.013

# Biokinetics of paralytic shellfish toxins in the green-lipped mussel, *Perna viridis*

K.N. Yu [a,*], Raymond W.M. Kwong [b], Wen-Xiong Wang [b], Paul K.S. Lam [c]

[a] *Department of Physics and Materials Science, City University of Hong Kong, Tat Chee Avenue, Kowloon, Hong Kong*
[b] *Department of Biology, Hong Kong University of Science and Technology (HKUST), Clear Water Bay, Kowloon, Hong Kong*
[c] *Department of Biology and Chemistry, City University of Hong Kong, Tat Chee Avenue, Kowloon, Hong Kong*

Paralytic shellfish toxins (PSTs) are a group of natural toxins produced by some species of phytoplankton dinoflagellates. Marine molluscs including mussels are particularly susceptible to PST intoxification via exposing to the toxic dinoflagellates due to their suspension-feeding behavior. These toxins can be transferred within food webs. In addition to the economical loss and damage to the aquaculture industries, paralytic shellfish poisoning (PSP) due to the consumption of PSTs contaminated seafood has also posed a serious health hazard in many countries in recent decades.

In a previous paper (Kwong et al., 2006), we reported that the relative proportions of PSTs (e.g., C toxins/GTX toxins) between the mussels and the toxic dinoflagellates (to which the mussels were exposed) are different. The fate of toxins is complicated by various mechanisms, such as differential accumulation and retention, chemical or enzymatic transformation (Shimizu and Yoshioka, 1981; Sullivan et al., 1983; Oshima, 1995), bacterial conversion (Kotaki et al., 1985). Several toxin transformations have been identified and documented, including epimerization, reduction and hydrolysis. However, processes of toxin conversion and intoxification/detoxification occur simultaneously, thus making the direct measurements of toxin kinetics difficult. Although, PSTs concentrations have been assessed through dynamic modeling (Silvert and Cembella, 1995; Silvert et al., 1998; Li et al., 2005), extraction of information on biotransformation from such dynamic modeling has yet to be explored.

* Corresponding author. Tel.: +852 27887812; fax: +852 27887830.
*E-mail address:* peter.yu@cityu.edu.hk (K.N. Yu).

The objective of the present paper is to employ a mathematical model to assess the PSTs in the mussel *Perna viridis*, because of its ecological and economic importance. We used *Alexandrium fundyense* (clone 1719) as the primary source of toxins due to its relatively high toxicity. The dynamic model provides quantitative prediction on toxin concentrations in the organisms at different times. Moreover, an attempt has been made to employ the detoxification rates derived for the uptake and depuration phases to reconstruct the biotransformation scenarios.

The detailed experimental design, toxin extraction and analytical procedures have been described in a previous paper (Kwong et al., 2006). Briefly, we exposed toxic dinoflagellate *A. fundyense* to the mussels *P. viridis* for 7 days, followed by 3 weeks depuration. The mussels were dissected into gills, hepatopancreas, gills, and foot and adductor muscle. After extraction, the toxins were quantified by high-performance liquid chromatography with post-column fluorescence derivatization (HPLC–FLD).

The model employed in this study followed that proposed by Silvert and Cembella (1995) for the uptake phase:

$$\frac{dC}{dt} = I - \lambda C \tag{1}$$

where $C$ is the concentration of toxin in the mussel, $I$ is the ingestion rate and $\lambda$ is the detoxification rate. Separate measurements were made for the toxin concentrations in the gills, viscera, hepatopancreas, adductor muscle and foot, but simultaneous studies of biokinetics among all these compartments seem too complex. Therefore, for a preliminary study, we have combined the measurements for all the compartments into a single "combined" compartment. The differential equation governing the time-dependent toxin concentrations in this combined compartment during the uptake phase is then given by Eq. (1) above. Similarly, the differential equation during depuration is given by

$$\frac{dC}{dt} = -\lambda C \tag{2}$$

The time-dependent toxin concentration in the combined compartment during uptake with the initial condition $C(t = 0) = 0$ is given by Eq. (3)

$$C = \frac{I}{\lambda}(1 - e^{-\lambda t}) \tag{3}$$

On the other hand, the time-dependent toxin concentration in the combined compartment during depuration with the initial conditions (on day 7) $C(t = 7 \text{ days}) = C_0$

$$C = C_0 e^{-\lambda t} \tag{4}$$

The experimental data were fitted using user-defined expressions in the non-linear curve fit program of the Microcal™ Origin™ (Version 6.0) with the interested parameters as the user-defined parameters (Li et al., 2005). The fitted results for the combined-compartment of *P. viridis* are shown in Figs. 1–6 for C1, C2, GTX3, GTX4, STX and

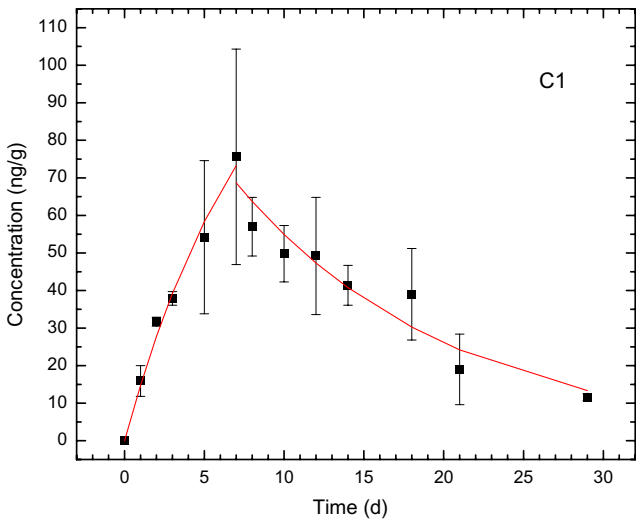


Fig. 1. Concentration (ng $g^{-1}$) of C1 toxin at different culture time in the combined compartment of *P. viridis*. Red line: best fit. Depuration started on the 7th day. Error bars represent ±1SD, $n = 3$. (For interpretation of the references to color in this figure legend, the reader is referred to the web version of this article.)

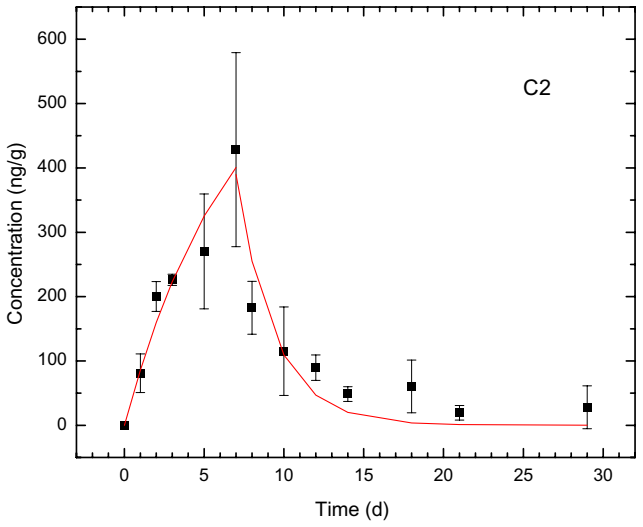


Fig. 2. Concentration (ng $g^{-1}$) of C2 toxin at different culture time in the combined compartment of *P. viridis*. Red line: best fit. Depuration started on the 7th day. Error bars represent ±1SD, $n = 3$. (For interpretation of the references to color in this figure legend, the reader is referred to the web version of this article.)

NeoSTX toxins, respectively. A summary of results for detoxification rates during uptake and depuration is given in Table 1. The detoxification rates are in general toxin specific. As mentioned above, the dynamic model with these detoxification rates provides quantitative prediction on the temporal variation of toxin concentrations in the mussel.

From the detoxification rates determined for the uptake and depuration phases, information on biotransformation between toxins can also be extracted. When there is no biotransformation or sequestration/binding, the detoxification rates of individual toxins during uptake and depuration are

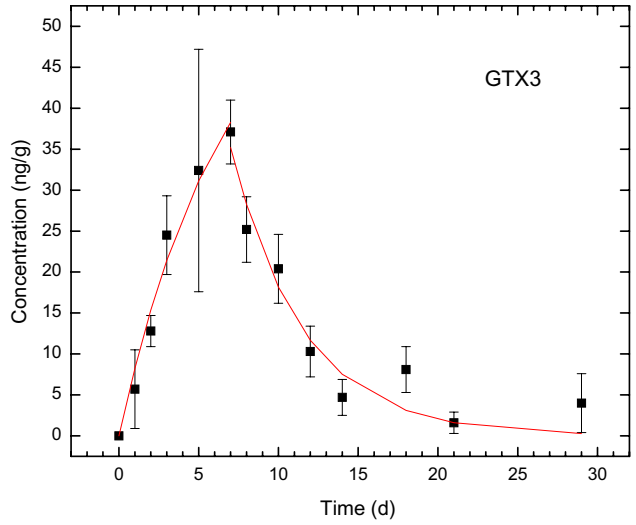


Fig. 3. Concentration (ng $g^{-1}$) of GTX3 toxin at different culture time in the combined compartment of *P. viridis*. Red line: best fit. Depuration started on the 7th day. Error bars represent ±1SD, $n = 3$. (For interpretation of the references to color in this figure legend, the reader is referred to the web version of this article.)

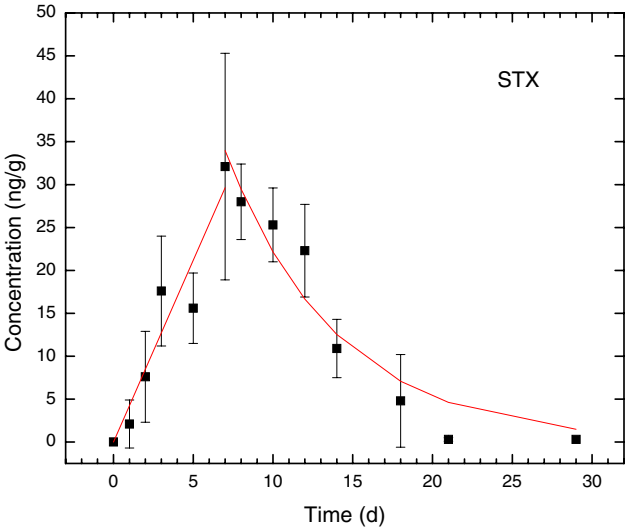


Fig. 5. Concentration (ng $g^{-1}$) of STX toxin at different culture time in the combined compartment of *P. viridis*. Red line: best fit. Depuration started on the 7th day. Error bars represent ±1SD, $n = 3$. (For interpretation of the references to color in this figure legend, the reader is referred to the web version of this article.)

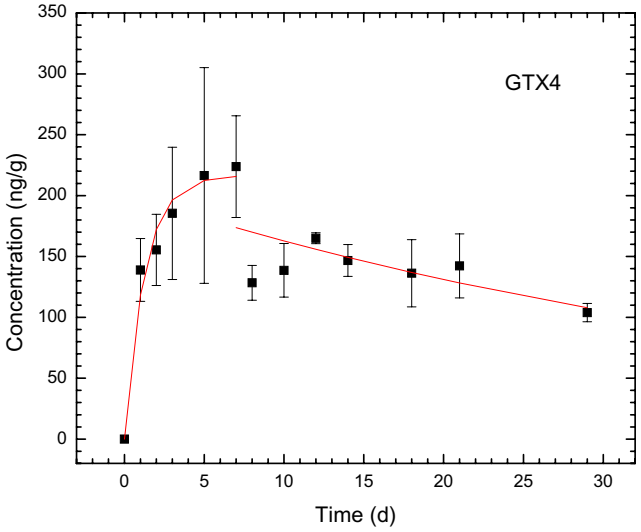


Fig. 4. Concentration (ng $g^{-1}$) of GTX4 toxin at different culture time in the combined compartment of *P. viridis*. Red line: best fit. Depuration started on the 7th day. Error bars represent ±1SD, $n = 3$. (For interpretation of the references to color in this figure legend, the reader is referred to the web version of this article.)

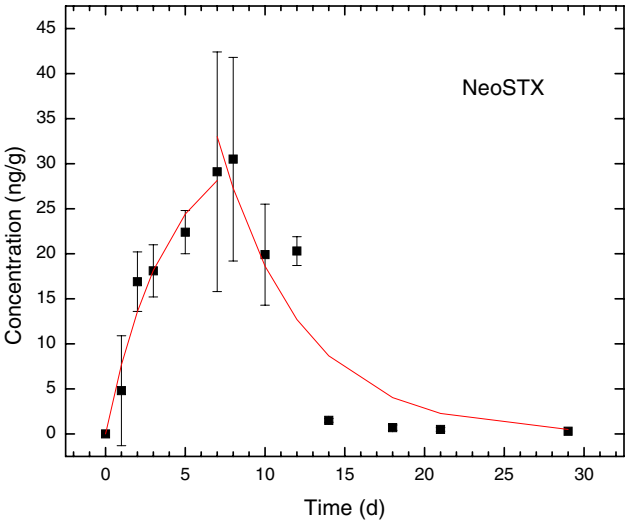


Fig. 6. Concentration (ng $g^{-1}$) of NeoSTX toxin at different culture time in the combined compartment of *P. viridis*. Red line: best fit. Depuration started on the 7th day. Error bars represent ±1SD, $n = 3$. (For interpretation of the references to color in this figure legend, the reader is referred to the web version of this article.)

expected to be similar. While, a lower detoxification rate during depuration (when compared to that during uptake) can be a result of sequestration/binding, a significantly higher detoxification rate during depuration can conceivably be viewed as an indicator for the occurrence of biotransformation. There can be two plausible causes for such a higher detoxification rate during depuration, namely,

(1) there is biotransformation from the toxin being considered to another toxin, through a mechanism with

Table 1
Summary of detoxication rates ($\lambda$) (in $d^{-1}$) for different toxins in the mussel during uptake and depuration

| | Uptake | Depuration |
|---|---|---|
| C1 | 0.124 ± 0.042 | 0.074 ± 0.012 |
| C2 | 0.149 ± 0.089 | 0.424 ± 0.110 |
| GTX3 | 0.153 ± 0.064 | 0.221 ± 0.037 |
| GTX4 | 0.791 ± 0.148 | 0.022 ± 0.011 |
| STX | Linear | 0.143 ± 0.025 |
| NeoSTX | 0.259 ± 0.093 | 0.191 ± 0.050 |

the transformation rate increasing on a time scale not significantly shorter than the uptake period; and

(2) there is biotransformation from a precursor toxin which is also biotransformed to a third toxin at a higher rate during depuration.

From the results shown in Table 1, we see that the detoxification rates during uptake and depuration are significantly different for C1, C2, GTX3, GTX4 and STX toxins, but not significantly different for the NeoSTX toxin. Therefore, we will not discuss the case for the NeoSTX toxin in the following. Using the above argument, we suggest that biotransformation has occurred for the C2, GTX3 and STX toxins.

The biotransformation for the C2 toxin might be explained by the epimerization between the C1/C2 toxin epimer pair, where such a conversion from a less stable β-epimer to a more stable α-epimer were commonly observed in bivalves (Oshima, 1995). This biotransformation is also supported by the fact that the C1 toxin has a lower detoxification rate during depuration.

The case for the STX toxin is particularly interesting, because the detoxification rate derived for the uptake phase is zero, i.e., the uptake is linear with time. This will almost exclude the possibility (1) described above that the biotransformation from STX to another toxin can explain the higher detoxification rate during depuration. We therefore focus on the possibility (2). From Table 1, biotransformations from C2 and/or GTX3 toxins to the STX toxin are feasible. However, there seems to be no direct paths for such biotransformations. A possibility is that the GTX3 toxin is first transformed to the GTX2 toxin through epimerization, which is then transformed to the STX toxin through reduction. The GTX2 toxin is likely to be transformed to STX with a very short time scale in the mussel, which is inferred from the fact that the *Alexandrium* cells contained a high ratio of GTX2/GTX3, but we were unable to detect GTX2 in the mussel samples (Kwong et al., 2006). It is also known that the C2 toxin can be converted into GTX3 toxin under acidic conditions. At the same time, as explained in the last paragraph, the C2 toxin is also biotransformed to the C1 toxin through epimerization. In this way, the C2 toxin can be viewed as a precursor for the STX toxin (through conversion to GTX3 and then GTX2), which is also biotransformed to a third toxin (C1 toxin) at a higher rate during depuration.

For the case of the GTX4 toxin, considering that the involved concentrations are significantly higher for this toxin, the small detoxification rate during depuration is not due to biotransformations from other toxins, and is likely due to sequestration/binding of the toxin itself.

In the present paper, we have explored the possibility of using the detoxication rates for different toxins in the mussel *P. viridis* during uptake and depuration to indicate the presence of biotransformation. In particular, we have proposed a significantly higher detoxification rate during depuration as an indicator for the occurrence of biotransformation. By using such an indicator, we suggest that in the mussel *P. viridis*, the C2 toxin is biotransformed to C1 toxin through epimerization and to GTX3 toxin under acidic conditions; and that the GTX3 toxin is first transformed to the GTX2 toxin through epimerization and then to the STX toxin through reduction. The model and the proposed indicator can be employed for experiments with other marine organisms. It is desirable that the dynamics of saxitoxins are verified with studies involving the toxins individually, which will be performed in future research. When the data are sufficient, study of biotransformation of toxins among different compartments of the same organism can also be possible. However, in such cases, much more complicated multi-level and multi-compartment models are needed.

## Acknowledgements

This study was supported by the Areas of Excellence Scheme established under the University Grants Committee of the Hong Kong SAR (Project No. AoE/P-04/2004).

## References

Kotaki, Y., Oshima, Y., Yasumoto, T., 1985. Bacterial transformation of paralytic shellfish toxins. In: Anderson, D.M., White, A.W., Baden, D.G. (Eds.), Toxic Dinoflagellates. Elsevier Science Publishers, New York, pp. 287–292.

Kwong, R.W.M., Wang, W.-X., Lam, P.K.S., Yu, K.N., 2006. The uptake, distribution and elimination of paralytic shellfish toxins in mussels and fish exposed to toxic dinoflagellates. Aquat. Toxicol. 80, 82–91.

Li, A.M.Y., Yu, K.N., Hsieh, D.P.H., Wang, W.-X., Wu, R.S.S., Lam, P.K.S., 2005. Uptake and depuration of paralytic shellfish toxins in the green-lipped mussel, *Perna viridis*: a dynamic model. Environ. Toxicol. Chem. 24, 129–135.

Oshima, Y., 1995. Chemical and enzymatic transformation of paralytic shellfish toxins in marine organisms. In: Lassus, P., Arzul, G., Erard, E., Gentien, P., Marcaillou, C. (Eds.), Harmful Marine Algal Blooms. Lavoisier/Intercept, Paris, pp. 475–480.

Shimizu, Y., Yoshioka, M., 1981. Transformation of paralytic shellfish toxins as demonstrated in scallop homogenates. Science 212, 547–549.

Silvert, W.L., Cembella, A.D., 1995. Dynamic modeling of phycotoxin kinetics in the blue mussel, Mytilus edulis, with implications for other marine invertebrates. Can. J. Fish Aquat. Sci. 52, 521–531.

Silvert, W., Bricelj, M., Cembella, A., 1998. Dynamic modeling of PSP toxicity in the surfclam (Spisula solidissima). In: Reguera, B., Blanco, J., Fernandez, M.L., Wyatt, T. (Eds), Harmful Algae, Xunta de Galicia and IOC of UNESCO, Santiago de Compostela, pp. 437–440.

Sullivan, J.J., Iwaoka, W.T., Liston, J., 1983. Enzymatic transformation of PSP toxins in the littleneck clam (*Protothaca staminea*). Biochem. Biophys. Res. Commun. 144, 465–472.

0025-326X/$ - see front matter © 2007 Elsevier Ltd. All rights reserved.
doi:10.1016/j.marpolbul.2007.02.007